

## CHAPTER 3

### Hydration Dynamics at Fluorinated Protein Surfaces

This chapter first appeared as an article in *Proceedings of the National Academy of Sciences, USA*: Oh-Hoon Kwon, Tae Hyeon Yoo, Christina M. Othon, James A. Van Deventer, David A. Tirrell, and Ahmed H. Zewail. *Proc. Natl. Acad. Sci. USA* **2010**, 107, (40) 17101-17106.

## Abstract

Water-protein interactions dictate many processes crucial to protein function including folding, dynamics, interactions with other biomolecules, and enzymatic catalysis. Here we examine the effect of surface fluorination on water-protein interactions. Modification of designed coiled-coil proteins by incorporation of 5,5,5-trifluoroleucine or (4*S*)-2-amino-4-methylhexanoic acid enables systematic examination of the effects of side-chain volume and fluorination on solvation dynamics. Using ultrafast fluorescence spectroscopy, we find that fluorinated side chains exert electrostatic drag on neighboring water molecules, slowing water motion at the protein surface.

## Introduction

The past decade has witnessed substantial expansion in the number and diversity of noncanonical amino acids that can be incorporated into recombinant proteins expressed in bacterial cells (1-3). Fluorinated amino acids have drawn special attention (4-16) because of the unusual solubility properties of fluorinated hydrocarbons. Several independent studies have shown that fluorination of coiled-coil and helix-bundle proteins leads to enhanced stability with respect to thermal or chemical denaturation (6-12), an effect attributed to the hyperhydrophobic and fluorophilic character of fluorinated amino acid side chains.

Although both classes of compounds are hydrophobic, hydrocarbons and fluorocarbons differ in important ways (17-22). The high electronegativity of fluorine renders the C-F bond both strongly polar and weakly polarizable (17, 21, 22). The dipole associated with the C-F bond exerts strong inductive effects on neighboring bonds (23)

and can form reasonably strong electrostatic interactions with ionic or polar groups when the two moieties are appropriately positioned. The hydrophobic character of fluorinated compounds has been described as “polar hydrophobicity (17),” and is believed to play important roles in organic and medicinal chemistry. Furthermore, the C-F bond is significantly longer than the C-H bond, and the calculated volume of the trifluoromethyl group is about twice that of a methyl group (20). The studies described here constitute an attempt to understand more fully the interaction of water with fluorinated molecular surfaces, and to provide a sound basis for the use of fluorinated amino acids in the engineering of proteins with unique and useful physical properties.

The hydration layer adjacent to protein surfaces exhibits properties different from those of bulk water; the more rigid and denser structure of the hydration layer plays a crucial role in protein structure, folding, dynamics, and function (24-26). Elucidation of the dynamic features of this region, on the timescales of atomic and molecular motion, is essential in understanding protein hydration. In the past decade, the knowledge of hydration on protein surfaces has been extensively expanded by studying the dynamic properties of biological water for various proteins containing tryptophan (Trp) or synthetic fluorescent amino acids as local probes; the results have revealed multicomponent relaxation dynamics spanning a wide range of timescales (25, 27-29). The nature of the protein hydration layer can be affected not only by the topographic and electrostatic properties of the protein surface (24), but also by the physical and chemical properties of individual surface-exposed residues (27, 30). In view of the unique properties of the C-F bond and of fluorocarbon–water interfaces (23, 31), we anticipated that fluorinated amino acid side chains might exhibit unusual hydration behavior. Here

we report studies of local hydration dynamics at fluorinated protein surfaces by monitoring the time-dependent fluorescence Stokes shifts of surface-exposed Trp residues in coiled-coil proteins with 5,5,5-trifluoroleucine (Tfl, **1**; scheme 3.1) residues adjacent to the probe. The results are compared to the hydration dynamics at hydrogenated protein surfaces with Leu (**2**) or (4*S*)-2-amino-4-methylhexanoic acid (homoisoleucine, Hil, **3**) adjacent to the Trp probe. Hil has approximately the same volume as Tfl (20, 21), and although the shapes of the residues differ, the nearly identical side-chain volumes of Tfl and Hil allow us to differentiate changes due to fluorination from those that result from the increase in side-chain volume that accompanies replacement of Leu (scheme 3.1).

## Results

**Coiled-coil protein system.** The coiled-coil protein A1 (figure 3.1 A and B) was used as a model system to examine the effects of fluorinated amino acids on local hydration dynamics. The primary structure of A1 contains six copies of a heptad repeat  $(abcdefg)_n$ , where positions *a* and *d* are occupied by hydrophobic amino acids. Self-association of the peptide juxtaposes the *a* and *d* positions and results in the formation of a hydrophobic core. Fluorinated Leu analogues have previously been incorporated into the *d* positions of A1; the resulting proteins exhibited improved resistance to thermal and chemical denaturation with minimal differences in secondary structure (9, 11, 12). In this work, the surface-exposed Asp residue at the *f* position of the third heptad (position 34) was replaced by Trp, which serves as a fluorescence probe (figure 3.1C). The Trp variant of A1 was designated A1m. In order to examine the effects of fluorinated analogues on the local hydration

dynamics, a Leu codon was introduced at one of two positions within A1m. Mutation of a serine residue at the *c* position of the third heptad (position 31) yielded a variant of A1 designated S31L (figure 3.1D), while replacement of an alanine residue at position *b* of the fourth heptad (position 37) gave the A1 variant A37L (figure 3.1E). Each protein was expressed in Tfl, Leu, and Hil form, yielding a total of nine different proteins that were examined in detail (see (32) for nomenclature).

**Characterization of global structure.** Analysis of each protein showed that the overall structural properties of the molecules were generally insensitive to genetic mutations and incorporation of noncanonical amino acids. Circular dichroism spectroscopy indicated that all nine proteins were helical, as determined from the molar ellipticity at 222 nanometers (figure 3.2) (33); an analysis with K2D2 software showed that the helicities of individual proteins range between approximately 40% and 48% (34). These results are consistent with the design of the A1 protein (35), in which approximately half of the amino acids are located within the heptad repeats expected to form  $\alpha$ -helical secondary structure. The oligomerization states of the protein samples were determined by sedimentation velocity analysis (figure 3.3). Although A1 forms dimers and tetramers at neutral pH (11), the variants examined in this study form trimers or hexamers under mildly acidic conditions (pH 4). We suggest that protonation of Glu side chains at the *e* and *g* positions (figure 3.1A) of the proteins decreases the density of negative charges adjacent to the hydrophobic core and promotes formation of larger helical aggregates at pH 4. A1m, in which the single Trp residue occupies a surface-exposed position, is predominantly trimeric in Leu-, Tfl-, and Hil-forms, with a small fraction of hexamers

(see figure 3.3). The majority of the S31L samples are present as hexamers, while the A37L samples appear to contain mixtures of trimers and hexamers.

**Characterization of local structure.** The steady-state fluorescence emission spectrum of Trp depends on the extent of exposure of the Trp side chain to water (36). All nine protein samples showed emission maxima between 349 and 352 nm, close to that of free Trp at 353 nm (table 3.1 and figure 3.4). These observations indicate that the Trp residues are exposed to the aqueous environment (consistent with the original design), and not involved in oligomerization of the proteins. In addition, the steady-state UV-visible absorption and steady-state fluorescence emission spectra of each mutant containing Leu were nearly identical to the spectra of the corresponding mutant when it contained Tfl or Hil (figure 3.4), further confirming that perturbation of the protein structure upon replacement of Leu by Tfl or Hil was minimal.

The mobility of the probe residue was explored in each protein by measuring fs-resolved depolarization dynamics (figure 3.5). The anisotropic dynamics were found to consist of three components: ultrafast ( $\leq 500$  fs), intermediate (20–80 ps), and slow ( $\geq 2$  ns) decays. The ultrafast decays are attributed to fast internal conversion between the first two excited singlet states ( $^1L_a$  and  $^1L_b$ ) of Trp, the intermediate decays to local wobbling motions of Trp, and the slow decays to tumbling motions of the proteins (28, 37). Similar values for the wobbling motions ( $\phi_{\text{Trp}}$ ) and their cone semiangles ( $\theta$ ) were observed for each series of S31L and A37L proteins (table 3.1); see material and methods for details.

Both mutation of residues around Trp and fluorination of the protein hydrophobic core can affect the environment of the probe and change the protein structure and/or the

dynamic properties of the hydration layer. In many cases these properties are related to one another. The minimal change in the steady-state fluorescence spectrum caused by replacement of Leu by Tfl or Hil suggests similar features of the hydration region probed by Trp (e.g., the effective number of water molecules in the hydration shell). In addition, the similarity of the Trp wobbling angle of the Leu-, Tfl-, and Hil-forms of the proteins suggests similar organization and flexibility of neighboring residues around the probe (28). All these features make it possible to compare the dynamic properties of protein hydration for most of the proteins in the A1m, S31L, and A37L proteins containing Leu, Tfl, and Hil. For A1m-H, we note that the wobbling angle of Trp was found to be  $33^\circ$ , which is significantly higher than the  $17^\circ$ – $21^\circ$  wobbling angles determined for all of the other proteins. This result indicates that the organization of local residues or the flexibility of the local Trp environment in A1m-H differs from that in the other proteins, despite the lack of global structural changes observed by circular dichroism or sedimentation velocity measurements. The abnormal behavior of the A1m-H variant is also observed in the fluorescence lifetime measurements. Every protein except A1m-H displayed a short-lifetime component of a few hundred picoseconds, present at all wavelengths. These types of quenching processes have been attributed to Trp interactions with nearby charged residues (38-40), and the absence of such a feature in A1m-H again indicates that this protein has a local structure different from those of the other eight proteins. The perturbation of local structure and, thus, local solvent exposure can result in different hydration dynamics, making it unreliable to compare the dynamics of A1m-H to those of the other A1m proteins. Accordingly, the dynamics obtained for A1m-H were not used in the analysis that follows. Small shifts in the fluorescence emission maximum

and Trp wobbling angle were observed for A37L-L as compared to A37L-T and A37L-H (see table 3.1 and figure 3.4). These differences may be significant enough to alter the local environment surrounding the Trp probe, potentially complicating assignment of changes observed in the hydration dynamics to a particular effect (e.g., changes in an amino acid close to Trp). Despite these concerns, the dynamics results for A37L-L remain consistent with the conclusions of the paper (see below).

Our stringent standards for comparison of hydration dynamics between modified proteins require that there be (i) no global change in protein structure as measured by circular dichroism spectroscopy and sedimentation velocity measurements; (ii) no change in solvent exposure as measured by steady-state fluorescence maximum ( $\pm 1$  nm); and (iii) no change in local protein structure or flexibility as measured by fluorescence anisotropy ( $\pm 1^\circ$ ). Seven of the nine proteins prepared in this study met all of these criteria, and an additional protein, A37L-L, displayed changes just outside the margin of error. Only one protein, A1m-H, showed changes significant enough to require us to disregard the hydration measurements observed. Given the subtle effects of the chemical environment on hydration dynamics, we will compare hydration results only within protein families. Thus, our strongest conclusions will be drawn from observations made on the S31L protein variants, and the data for A1m and A37L will be used as corroborating evidence.

**Ultrafast hydration dynamics.** To investigate hydration dynamics at the protein surfaces, we utilized a methodology developed by Zhong and coworkers for the reconstruction of femtosecond-resolved fluorescence spectra (28, 41). As an example,

figure 3.6A shows several representative femtosecond-resolved fluorescence transients recorded for A1m-T. The overall decay dynamics is retarded compared to that of free Trp in buffer solution. Details of the results for all the protein samples are presented in table 3.1. The hydration dynamics of the proteins were well represented by triple-exponential decays with distinctive timescales of 0.2–0.8, 1.4–6.1, and 10–61 picoseconds. Relaxation occurring on a time scale of a few hundred femtoseconds to several picoseconds is attributed to fast librational/rotational motions of bulk-type and local water molecules around Trp. Observation of the fs component suggests that the Trp probe in the test proteins is neither crowded by neighboring residues nor protected from exposure to water (27, 28, 42). The slowest phase of hydration dynamics (on the timescale of tens of picoseconds) is collective water network rearrangement coupled to protein fluctuation dynamics (27, 42-44).

Several key features of the results (figure 3.7 and table 3.1) are summarized as follows. First, S31L-T and A37L-T, in which Trp lies close to Trp as well as in the hydrophobic core, showed slower hydration dynamics than their His and Leu counterparts, indicating that the fluorinated surface of the protein slows down the hydration dynamics. For S31L-T, the timescales of local and collective water motions ( $\tau_2$  and  $\tau_3$ , respectively) are increased by 2–5 times (3.0 and 48 ps) from those of S31L-H (1.4 and 10 ps). The overall solvation of S31L-T is slower than that of S31L-L as well. However, this difference is manifested as an increase in the contribution of the  $\tau_3$  component to the overall solvation of Trp. The 70% increase of the relaxation energy ( $333 \text{ cm}^{-1}$ ) of the slowest component ( $E_3$ ) compared to that of the nonfluorinated S31L-L ( $194 \text{ cm}^{-1}$ ) is an indication of the dramatic slowing of hydration dynamics near the

fluorinated surface. For A37L-T,  $\tau_2$  and  $\tau_3$  are also retarded to a greater extent (3–5 times slower) than those for A37L-H. These results suggest that replacement of Leu by Trp increases the residence time of water molecules near the Trp probe and/or the number of water molecules influenced by the amino acid side chain.

Second, S31L-H and A37L-H showed similar or even faster hydration than their Leu counterparts. This result indicates that in the comparison between hydrocarbon residues, increasing the hydrophobic surface area results in faster motion of water molecules around the residue. It should be noted that, for the S31L series, hydration is greatly accelerated when Leu is replaced with His. This pronounced hydrophobic effect (due to the increase in the size of the residue) on the hydration is counteracted by fluorination of leucine, resulting in slowing dynamics for S31L-T. On the other hand, for A37L, increasing the size of the hydrophobic surface does not appear to affect the hydration dynamics as greatly. Therefore, the retardation of the dynamics upon fluorination is much more pronounced for A37L-T than for the corresponding fluorination of S31L. Finally, A1m-L and A1m-T, which differ from one another only in the nature of their hydrophobic cores, exhibited almost identical hydration dynamics. Fluorination of the hydrophobic core of a helix-bundle protein can affect protein dynamics (45). However, the nearly identical hydration dynamics for A1m-L and A1m-T spanning a few hundred picoseconds indicates that modification of the hydrophobic core of A1m does not affect protein motions that are coupled to local hydration dynamics at the surface of the protein on the timescales examined here (46).

## Discussion

Protein surfaces are heterogeneous, consisting of polar, hydrophilic, and hydrophobic residues, and it is intriguing to consider how the heterogeneous surface chemistry affects the behavior of water molecules in the protein hydration layer. Head-Gordon and coworkers have reported heterogeneous water dynamics in the first hydration shell of model peptides (*N*-acetyl-leucinemethylamide and *N*-acetyl-glycinemethylamide), with faster water motions near the hydrophobic side chains than near the hydrophilic backbone (47, 48). Similar results have been reported for molecular dynamics simulation studies of a folded  $\beta$ -hairpin peptide (30). In addition, Qiu et al. showed that mutation of charged or polar residues of the enzyme staphylococcal nuclease into more hydrophobic residues (Ala), resulted in faster hydration dynamics; this result was attributed to the lack of strong interaction between the charges (or dipoles) of the mutated protein and the surrounding water (27). This observation can be understood in that the elimination of specific interactions between hydrophobic residues and water molecules causes a lower number of hydrogen bonds between water and a hydrophobic surface compared to those near a hydrophilic surface, thus allowing water molecules to reorient more freely. Computational studies have suggested that water layers adjacent to extended hydrophobic surfaces of low curvature are of lower density than those around hydrophilic and small hydrophobic molecules, and are dynamic rather than static (49-56). X-ray reflectivity experiments indicate submonolayer water depletion at hydrocarbon and fluorocarbon surfaces (57). Our observation of accelerated hydration dynamics around larger His residues as compared to the smaller Leu is consistent with these experimental and computational results, supporting the idea that water molecules neighboring hydrophobic

side chains in the hydration layer of proteins are more dynamic than those around polar or hydrophilic residues.

Even though a simple comparison suggests that Tfl should be more hydrophobic than Leu by virtue of its larger surface area, introduction of a Tfl residue adjacent to the Trp probe caused retardation of the local hydration dynamics, in contrast to the results obtained when Leu was replaced with Hil (figure 3.7). These results suggest that hydration dynamics around fluorinated amino acid side chains cannot be explained exclusively by the increase in residue size. The C-F bond is assumed not to be involved in hydrogen bonding with liquid water, largely because of its low polarizability (17). However, replacement of Leu by Tfl introduces a strong dipole at the fluorinated protein surface. Lee and coworkers have shown that introduction of  $\text{CF}_3$  groups reduces the contact angle of water on self-assembled alkanethiol monolayers (23), an effect that they attribute to dipolar interactions. Our results suggest that such dipolar interactions can also slow water motions at fluorinated molecular surfaces.

Fluorinated compounds are more hydrophobic than hydrogenated compounds of equal carbon number (4, 5, 17-21), and the increase in hydrophobic character of fluorocarbons has been ascribed to their increased molecular size (18, 58). This interpretation appears to be consistent with the observation that the melting temperature of A1-Tfl is 13 °C higher than that of A1-Leu (11), while  $T_m$  for A1-Hil is increased by 17 °C in comparison to A1-Leu. However, the results reported here clearly indicate that the chemical nature of the protein surface dictates the dynamics of solvent-protein interactions, and that size effects alone cannot explain the altered solvation dynamics observed at fluorinated protein surfaces.

## Conclusions

The results reported here show that fluorinated amino acids influence hydration dynamics at protein surfaces in a manner quite different from their hydrogenated counterparts. In general, water-protein interactions dictate many processes crucial to protein function including folding, dynamic motions, interactions with other biomolecules, and enzymatic catalysis (26). The slower timescales of hydration dynamics observed near fluorinated residues in proteins suggest that some of the water-mediated processes listed above may be changed upon fluorination. Tailoring the dynamics of protein-water interactions by the introduction of fluorinated residues may yield proteins with functional properties, such as binding, molecular recognition, or catalytic activities, that cannot be achieved with the canonical amino acids. Understanding hydration dynamics at fluorinated molecular surfaces is a critical step toward exploiting the properties of fluorine in biological systems.

## Materials and Methods

**Summary of protein expression and characterization.** A1 variants A1m, S31L, and A37L were expressed in 2×YT medium (which contains Leu) to yield proteins A1m-L, S31L-L, and A37L-L, respectively, in Leu-free M9 minimal medium (12.8 g/L  $\text{Na}_2\text{HPO}_4 \cdot 7\text{H}_2\text{O}$ , 3 g/L  $\text{KH}_2\text{PO}_4$ , 0.5 g/L NaCl, 1 g/L  $\text{NH}_4\text{Cl}$ ) supplemented with 19 canonical amino acids plus Tfl to give A1m-T, S31L-T, and A37L-T, and in Leu-free M9 medium supplemented with 19 canonical amino acids plus Hil to give A1m-H, S31L-H, and A37L-H. The proteins were purified under denaturing conditions and dialyzed against 10 mM acetate (pH 4)/100 mM NaCl. The extent of replacement of Leu by Tfl in A1m-T,

S31L-T, and A37L-T, was determined by amino acid analysis to be 90%–91%. Leu replacement by His in A1m-H, S31L-H, and A37L-H was analyzed by liquid chromatography tandem mass spectrometry and determined to be at least 90% (figure 3.8). See below for further details of expression, purification, and incorporation analysis.

**Summary of steady-state measurements.** Circular dichroism spectra were recorded on an Aviv 62DS spectropolarimeter (Lakewood, NJ). Absorption spectra were collected using a Cary 500 UV-Vis spectrophotometer and a 0.05 mm path length cuvette. Steady-state fluorescence emission spectra were measured using a FluoroMax-2 fluorimeter (ISA-Spex).

**Summary of time-resolved fluorescence measurements.** The experimental apparatus for time-resolved measurements are detailed below. All fluorescence spectra and transients were obtained by the excitation of samples ( $\sim 550 \mu\text{M}$ ) at 295 nanometers. The lifetime components were obtained by global analysis of fluorescence transients collected using a time-correlated single photon counting spectrometer. All transients show additional multiple-exponential decay (at the blue side) and rise (at the red side) with time constants spanning from a few hundred femtoseconds to several tens of picoseconds. In order to extract hydration dynamics precisely, we reconstructed apparent and lifetime-associated time-resolved fluorescence spectra with eight or nine transients at different wavelengths covering the blue and the red sides (figure 3.6B). By fitting these spectra to lognormal functions, we traced the time-dependent apparent emission maxima ( $\nu_s$ ) and lifetime-associated emission maxima ( $\nu_l$ ) as plotted in figure 3.6C. Using  $\Delta\nu(t) = \nu_s(t) - \nu_l(t)$ , we

correlated the extracted time-dependent spectral shift,  $\Delta\nu(t)$ , to the hydration energy relaxation,  $\Delta E_s$  (figure 3.7).

**Materials.** All restriction enzymes were purchased from New England Biolabs (Beverly, MA). D,L-5,5,5-trifluoroleucine (Tfl) was purchased from Oakwood Products (West Columbia, SC). DNA oligomers were synthesized at Qiagen (Valencia, CA) or Integrated DNA Technologies (Coralville, IA). (4*S*)-2-amino-4-methylhexanoic acid (homoisoleucine, Hil) was prepared according to the methods of O'Donnell and Eckrich (59) and Dorizon and coworkers (60).

**Plasmid construction.** An EcoRI/HindIII fragment of pQEA1 (11) containing the A1 coding sequence was ligated into EcoRI/HindIII-digested pQE-80L (Qiagen) to yield pQE-80L/A1. The Asp residue at position 34 of A1 was mutated to Trp by site-directed mutagenesis. The resulting plasmid was designated pQE-80L/A1m. A Leu codon was introduced into either position 31 or position 37, yielding pQE-80L/S31L and pQE-80L/A37L, respectively. Plasmid pA1EL (12), which encodes both the protein A1 and a constitutively expressed leucyl-tRNA synthetase (LeuRS), was mutated using similar site-directed mutagenesis techniques. A Trp codon was introduced first at position 34 of A1, yielding pA1mEL. Introduction of leucine codons into either position 31 or position 37 resulted in the plasmids pS31LEL and pA37LEL, respectively.

**Expression of fluorinated proteins.** M9 medium supplemented with 0.4% glucose, 3.5 mg/L thiamine, 1 mM MgSO<sub>4</sub>, 0.1 mM CaCl<sub>2</sub>, 20 amino acids (40 mg/L), and 200 mg/L

ampicillin was inoculated 1:50 with an overnight culture (M9) of *Escherichia coli* strain DH10B transformed with pQE-80L/A1m, pQE-80L/ S31L, or pQE-80L/A37L and grown at 37 °C with shaking. After each culture reached  $OD_{600} = 0.9-1.0$ , the cells were harvested by centrifugation ( $6000 \times g$ , 4 °C, 6 min) and washed twice with cold 0.9% NaCl. The cell pellets were resuspended in M9 medium containing 19 amino acids (no Leu) and 1 mM Tfl. Protein expression was induced 10 min after the medium shift by addition of IPTG to a final concentration of 1 mM. After 3 h, the cells were harvested by centrifugation ( $6000 \times g$ , 4 °C, 10 min), and the cells were stored at -20 °C at least 12 h before purification. In the case of the protein S31L-T, one sample was made using the procedure for the production of proteins containing Hil described below.

**Expression of proteins containing homoisoleucine.** M9 medium supplemented with 0.4% glucose, 35 mg/L thiamine, 1 mM  $MgSO_4$ , 0.1 mM  $CaCl_2$ , 20 amino acids (40 mg/L), 200 mg/L ampicillin, and 35 mg/L kanamycin was inoculated 1:50 with an overnight culture (M9) of *E. coli* strain LAM1000 transformed with pREP4 and pA1mEL, pS31LEL, or pA37LEL at 37 °C with shaking. After each culture reached  $OD_{600} = 0.9-1.1$ , the cells were harvested by centrifugation ( $5000 \times g$ , 4 °C, 15 min) and washed three times with cold 0.9% NaCl. The cell pellets were resuspended in M9 medium containing 19 amino acids (no Leu) and 0.5 mM Hil. Protein expression was induced 15 min after the medium shift by the addition of IPTG to a final concentration of 1 mM. Cells were harvested by centrifugation ( $5000 \times g$ , 4 °C, 15 min), resuspended in Qiagen buffer B (8M urea, 100 mM  $NaH_2PO_4$ , 10 mM TrisCl, pH 8.0) and sonicated for 10 min total process time

with a pulse duration of 5 s and a wait duration of 5 s. The sonicated lysates were frozen at  $-80\text{ }^{\circ}\text{C}$  for at least 12 h before proceeding with purification.

**Expression of hydrogenated proteins.** Rich ( $2\times\text{YT}$ ) medium was used instead of supplemented M9 medium. When the culture reached  $\text{OD}_{600} = 0.9\text{--}1.0$ , IPTG was added to a final concentration of 1 mM. After 3 h, the cells were harvested by centrifugation ( $6000 \times g$ ,  $4\text{ }^{\circ}\text{C}$ , 10 min), and the cells were stored at  $-20\text{ }^{\circ}\text{C}$  at least 12 h before purification. In the case of S31L-L, one sample was expressed using the cell strain LAM1000 containing pREP4 and pS31LEL and harvested using the procedure used for the production of proteins containing Hil.

**Protein purification.** N-terminally histidine-tagged A1 variants were purified under denaturing conditions by affinity chromatography using Ni-NTA resin (Qiagen, Chatsworth, CA) according to the manufacturer's instructions. For proteins containing Hil and for one batch each of S31L-L and S31L-T, the lysates in Qiagen buffer B were thawed, sonicated, and then clarified using centrifugation ( $\sim 75,000 \times g$ ,  $25\text{ }^{\circ}\text{C}$ , 10 min). Imidazole was added to Qiagen buffer C (50 mM) and Qiagen buffer E (250 mM) in order to improve purification efficiency. The purified protein solutions were dialyzed against 10 mM sodium acetate (pH 4)/100 mM NaCl, and were concentrated by ultrafiltration (Amicon Ultra-15 devices, mwco: 10,000 or 3000, Millipore, Billerica, MA). The protein concentration was determined as measured by the absorbance at 280 nanometers of solutions, assuming extinction coefficients of  $5500\text{ M}^{-1}\text{ cm}^{-1}$  (61).

**Amino acid analysis and sedimentation velocity analysis.** Amino acid analysis of fluorinated proteins was performed at the W. M. Keck Facility at Yale University (New Haven, CT) on a Hitachi L-8900 amino acid analyzer (San Jose, CA) after hydrolysis at 115 °C in 70% formic acid. Sedimentation velocity analysis was performed at the National Analytical Ultracentrifugation Facility at the University of Connecticut (Storrs, CT) by using a Beckman XL-I Analytical Ultracentrifuge at 20 °C. The rotor was accelerated to 55,000 rpm, and interference scans were acquired at 1 min intervals for 7 h. The data were analyzed by using the program Sedfit (62) to obtain normalized  $c(s)$  versus sedimentation coefficient plots (figure 3.3).

**Mass spectrometry.** Liquid chromatography tandem mass spectrometry (LC/MS/MS) of proteins containing Hil or Tfl was performed at the Caltech Protein and Peptide Mass Analytical Laboratory. Trypsinized samples were subjected to liquid chromatography on an Eksigent (Dublin, CA) NanoLC-2D using a 6 cm long, 100  $\mu$ m diameter C18 column, followed by MS/MS on an Applied Biosystems (Foster City, CA) QStar XL instrument. Data were analyzed using Analyst QS software provided by Applied Biosystems. Hil or Tfl incorporation levels were estimated using information contained within extracting ion currents (XIC) of trypsin-digested protein samples. For a given sample, a peak corresponding to a peptide globally substituted with the noncanonical amino acid and coding for multiple leucines was identified, and the related peak corresponding to replacement at a fraction of the leucine positions was also identified. Determination of the ratio of the partially substituted to globally substituted peak areas allowed for the estimation of amino acid incorporation levels assuming that leucines in the fragment were

replaced statistically. An example calculation is shown in the subsection “LC/MS/MS amino acid incorporation estimates,” which can be found below.

**Time-correlated single-photon counting (TCSPC).** The protein samples were prepared at 55  $\mu\text{M}$  concentration in 10 mM acetate (pH 4)/100 mM NaCl solution. The TCSPC measurements were performed by using femtosecond pulses ( $<100$  fs) from a Ti-sapphire oscillator (Spectra-Physics, Mai Tai HP). Laser output, of which the repetition rate was attenuated from 80 to 8 MHz utilizing a pulse picker (Spectra-Physics, Model 3980-5), was tuned to 885 nanometers and frequency-tripled to 295 nanometers using a time-plate tripler (Minioptic Technology, TP-2000B) for selective excitation of Trp. The UV beam, vertically polarized using a half waveplate, was introduced to a sample chamber and focused onto the sample cell. The residual frequency-doubled beam from the tripler was directed to a photodiode to trigger a TCSPC system (PicoQuant GmbH, FluoTime 200). Typically, the energy of the excitation pulse (attenuated) at the sample was  $\sim 10$  picojoules. In a right-angle geometry, the emitted fluorescence was collected at a magic angle ( $54.7^\circ$ ) with respect to the vertically polarized excitation beam and focused into a MCP-PMT (Hamamatsu, R3809U), which is attached to a double monochromator. The photomultiplier tube signal was routed to a time-to-amplitude converter as a start signal followed by a constant fractional discriminator (PicoQuant GmbH, SPC 630). To avoid possible photobleaching and photodegradation, samples were kept stirring using a micro magnetic stirrer. In this configuration, the instrument response has a full width at half maximum of  $\sim 30$  ps. Multiexponential decays convoluted with instrumental response functions were analyzed using the FluoFit software package (PicoQuant).

**Femtosecond fluorescence upconversion.** The protein samples were prepared at 550  $\mu\text{M}$  concentration in 10 mM acetate (pH 4)/100 mM NaCl solution. An amplified Ti-sapphire laser system (Spectra-Physics, Hurricane X) was used, which produces  $\sim 110$  fs pulses centered at 805 nanometers (fundamental), with a 1 kHz repetition rate and a 0.8 millijoule energy. The output beam was split into equal parts to generate the pump and the gate pulse trains. For the pump, the fundamental light was used to pump an optical parametric amplifier (Spectra-Physics, OPA-800C), the infrared idler output of which was sum-frequency mixed with the residual fundamental in a 0.5 mm thick  $\beta$ -barium borate (BBO) crystal (type I), recompressed with a prism pair, and frequency-doubled to provide the 295-nanometers pulses in a 1.0 mm thick BBO crystal. The pump pulses were focused, with a 24 cm focal length lens, on the rotating circular cell (1 mm thickness) containing the sample. Typically, the energy of the pump pulse (attenuated) at the sample was  $\sim 200$  nJ. At these energies, the fluorescence signals from samples were linearly dependent on the pump energy. To check for sample degradation during experiments, fluorescence spectra were periodically measured right after the rotating cell by using a fiber-optic-coupled spectrometer (Acton Research, SpectraPro-300i) coupled to a charge-coupled device (Princeton Instruments, SpectruMM-256HB) before and after the collection of averaged transients for each sample. No difference between the spectra was observed.

The forward-scattered fluorescence from excited samples was collected and focused by two off-axis parabolic mirrors into a 0.5 mm thick BBO crystal. Cutoff filters were placed between the mirrors to reject scattered laser light and pass the desired fluorescence wavelengths. The gate pulses, attenuated to 23  $\mu\text{J}/\text{pulse}$ , passed through a computer-controlled optical delay line and were noncollinearly overlapped with the

fluorescence in the BBO crystal. After the crystal, the upconverted signal was separated from the gate beam and the fluorescence by using an iris, and was focused on the entrance slit of a 0.25 m double-grating monochromator (Jobin Yvon, DH10) equipped with a photomultiplier tube at the exit slit. Upconversion efficiency was maximized by angle-tuning of the BBO crystal. The upconverted fluorescence transients were taken at the magic angle ( $54.7^\circ$ ) of the pump polarization relative to the gate polarization, parallel to the acceptance axis of the upconversion crystal, in order to eliminate the influence of induced sample anisotropy on the signal. The photomultiplier output was amplified (Stanford Research Systems (SRS), SR445) and processed by a gated integrator (SRS, SR250). The temporal response of the instrument was typically 350–450 fs. The observed fluorescence transients were fit to theoretical functions, using a Scientist nonlinear least-squares fitting program (Micromath), for the convolution of the Gaussian instrument response function with a sum of exponentials. All experiments were carried out at an ambient temperature of  $\sim 24^\circ\text{C}$ , and all fluorescence transients were obtained by the excitation of samples at 295 nanometers.

For fluorescence anisotropy measurements, the pump-beam polarization was rotated either parallel or perpendicular to the acceptance axis of the upconversion crystal to collect the parallel ( $I_{\parallel}$ ) and perpendicular ( $I_{\perp}$ ) signals, respectively. These transients were used to construct time-resolved anisotropy:  $r(t) = (I_{\parallel} - I_{\perp}) / (I_{\parallel} + 2I_{\perp})$ . The results of the time-resolved anisotropy are shown in figure 3.5. The ultrafast depolarization time constant,  $\phi_1$ , attributed to fast internal conversion between the first two excited singlet states ( $^1L_a$  and  $^1L_b$ ) of Trp, varies dramatically with the time resolution. This process has a timescale of  $\sim 100$  fs (63, 64). The limited resolution of our current apparatus (350–450 fs) does not

allow us to fully resolve these dynamics and gives rise to a large uncertainty in the value of  $\phi_l$ . The variability of  $\phi_l$  will impact the fit of  $\phi_{\text{Trp}}$ . The uncertainty in the amplitude of the anisotropy,  $r_{\text{Trp}}$  and  $r_\infty$ , is not however affected by the limited time resolution of our data. Therefore we use the wobbling cone angle to reveal details about the local crowding near Trp. The wobbling cone angle is given by  $1 - r_{\text{Trp}}/(r_{\text{Trp}} + r_\infty) = [(3\cos^2q - 1)/2]^2$  (37), and only depends upon the amplitude of the tryptophan wobbling motion and the anisotropy due to the rotation of the molecule.

**LC/MS/MS amino acid incorporation estimates.** LC/MS/MS was used to estimate the replacement levels of leucine in some protein samples. Figure 3.8 depicts the total ion currents (TIC, figure 3.8A) and three extracted ion currents (XICs, figure 3.8B–D) from a digested A1m-H sample. The large peak in figure 3.8B corresponds to a peptide in which all of the Leu residues are replaced by Hil, the smaller peak in figure 3.8C corresponds to a mixture of two peptides containing one Leu and one Hil residue, and the very small peak in figure 3.8D corresponds to a peptide containing only Leu residues. The areas in the three XICs allow determination of the extent of incorporation of noncanonical amino acids in place of leucine. Assuming that there is a probability  $p$  of homoisoleucine substitution in place of leucine, the distribution of peak areas should correspond to the binomial distribution,

$$A[(1-p)^2 + 2(1-p)p + p^2], \quad (3.1)$$

where  $A$  is a multiplication factor equal to the total area of the three peaks and the three terms of the polynomial correspond to nonsubstituted, singly substituted, and doubly substituted peptides, respectively (the term for singly substituted peaks takes into account both positional isomers of singly substituted peptides). Because these three terms represent the only combinations of substitutions possible in the peptide, the relationship

$$(1 - p)^2 + 2(1 - p)p + p^2 = 1 \quad (3.2)$$

also holds. The ratio between two peaks in a peptide series depends only on the probability of incorporation and not on the value of  $A$ . Therefore, the ratio of two peaks from experimental data can be used in order to get an estimate of  $p$ . The ratio of the peak areas of singly substituted to doubly substituted peptides is

$$\frac{2(1 - p)p}{p^2}. \quad (3.3)$$

Rearranging the above expression,

$$\frac{2p - 2p^2}{p^2} = \frac{2(1 - p)p}{p^2} = X, \quad (3.4)$$

where  $X$  is the experimentally observable ratio of singly substituted to doubly substituted peptides. Solving for  $p$  gives

$$p = 0, \quad (3.5)$$

or

$$p = \frac{2}{X+2}, \quad (3.6)$$

with the root of interest being the nonzero root. Substituting for the ratio of peak areas gives an estimate of the incorporation level  $p$ .

In some cases, peaks corresponding to peptides containing three leucine or leucine analogs were observed and used to quantify incorporation levels. In these cases, the peak area distribution is represented by

$$A[(1-p)^3 + 3(1-p)^2 p + 3(1-p)p^2 + p^3], \quad (3.7)$$

with

$$(1-p)^3 + 3(1-p)^2 p + 3(1-p)p^2 + p^3 = 1. \quad (3.8).$$

Defining the ratio of doubly substituted to triply substituted peak area as  $X$ , substituting  $X$  into equation (3.8), and solving for  $p$  yields the nonzero root

$$p = \frac{3}{X+3}, \quad (3.9)$$

again enabling an estimation of the incorporation level of noncanonical amino acids in place of leucine. In some cases, the tandem mass spectrometry did not enable positive identification of all possible positional isomers of a peptide. For example, in some cases, only two out of three of the possible doubly substituted positional isomers containing three possible substitution locations were identified in the tandem mass spectrometry data. In these cases,  $X$  was multiplied by an appropriate factor to account for peptides that were not observed (again invoking the assumption of completely random incorporation). Using the above example, when only two out of three doubly substituted peptides could be identified,  $X$  was multiplied by a factor of 1.5 in order to estimate what the peak area ratio would have been with all three peaks present in equal weights. Using this methodology, the homoisoleucine-containing proteins used were found to have 90% or greater Hil in place of Leu, and the sample of S31L-T that was analyzed in this fashion contained approximately 99% Tfl in place of Leu. These results were obtained by examining three separate series of peptides from each protein sample. These peptides had the following sequences: AEIGDLNNTSGIR, GSHHHHHHGSMASGDLENEVAQLER, and SLEWEAAELEQK (A1m), LLEWEAAELEQK (S31L), or SLEWEALELEQK (A37L).

## **Acknowledgements**

We thank Professor Thomas Miller for helpful discussion, J. D. Fisk for synthesis of homoisoleucine, and the referees for their thoughtful comments on the original manuscript. This work is supported by National Institutes of Health (NIH) Grant GM62523, National Science Foundation (NSF) Grant DMR-0964886, Office of Naval

Research (ONR) Grant N00014-03-1-0793, a Samsung Scholarship (to T. H. Y.), and a National Defense Science and Engineering Graduate Fellowship (to J. A. V.).

## References

1. Budisa N (2006) *Engineering the Genetic Code: Expanding the Amino Acid Repertoire for the Design of Novel Proteins* (Wiley-VCH, Weinheim, Germany).
2. Link AJ, Mock ML, & Tirrell DA (2003) Non-canonical amino acids in protein engineering. *Curr. Opin. Biotechnol.* **14**, 603-609.
3. Xie JM & Schultz PG (2006) Innovation: a chemical toolkit for proteins - an expanded genetic code. *Nature Reviews: Molecular Cell Biology* **7**, 775-782.
4. Marsh ENG (2000) Towards the nonstick egg: designing fluororous proteins. *Chem. Biol.* **7**, R153-R157.
5. Yoder NC, Yuksel D, Dafik L, & Kumar K (2006) Bioorthogonal noncovalent chemistry: fluororous phases in chemical biology. *Curr. Opin. Chem. Biol.* **10**, 576-583.
6. Bilgicer B, Fichera A, & Kumar K (2001) A coiled coil with a fluororous core. *J. Am. Chem. Soc.* **123**, 4393-4399.
7. Jackel C, Salwiczek M, & Kokschi B (2006) Fluorine in a native protein environment - How the spatial demand and polarity of fluoroalkyl groups affect protein folding. *Angew. Chem. Int. Ed.* **45**, 4198-4203.
8. Lee KH, Lee HY, Slutsky MM, Anderson JT, & Marsh ENG (2004) Fluororous effect in proteins: De novo design and characterization of a four-alpha-helix bundle protein containing hexafluoroleucine. *Biochemistry* **43**, 16277-16284.

9. Montclare JK, Son S, Clark GA, Kumar K, & Tirrell DA (2009) Biosynthesis and stability of coiled-coil peptides containing (2S,4R)-5,5,5-trifluoroleucine and (2S,4S)-5,5,5-trifluoroleucine. *ChemBioChem* **10**, 84-86.
10. Son S, Tanrikulu IC, & Tirrell DA (2006) Stabilization of bzip peptides through incorporation of fluorinated aliphatic residues. *ChemBioChem* **7**, 1251-1257.
11. Tang Y, *et al.* (2001) Fluorinated coiled-coil proteins prepared in vivo display enhanced thermal and chemical stability. *Angew. Chem. Int. Ed.* **40**, 1494-1496.
12. Tang Y & Tirrell DA (2001) Biosynthesis of a highly stable coiled-coil protein containing hexafluoroleucine in an engineered bacterial host. *J. Am. Chem. Soc.* **123**, 11089-11090.
13. Montclare JK & Tirrell DA (2006) Evolving proteins of novel composition. *Angew. Chem. Int. Ed.* **45**, 4518-4521.
14. Wang P, Tang Y, & Tirrell DA (2003) Incorporation of trifluoroisoleucine into proteins in vivo. *J. Am. Chem. Soc.* **125**, 6900-6906.
15. Yoo TH, Link AJ, & Tirrell DA (2007) Evolution of a fluorinated green fluorescent protein. *Proc. Natl. Acad. Sci. U. S. A.* **104**, 13887-13890.
16. Yoo TH & Tirrell DA (2007) High-throughput screening for Methionyl-tRNA synthetases that enable residue-specific incorporation of noncanonical amino acids into recombinant proteins in bacterial cells. *Angew. Chem. Int. Ed.* **46**, 5340-5343.
17. Biffinger JC, Kim HW, & DiMugno SG (2004) The polar hydrophobicity of fluorinated compounds. *ChemBioChem* **5**, 622-627.
18. Gao JM, Qiao S, & Whitesides GM (1995) Increasing binding constants of ligands to carbonic-anhydrase by using greasy tails. *J. Med. Chem.* **38**, 2292-2301.

19. Jackel C & Kokschi B (2005) Fluorine in peptide design and protein engineering. *Eur. J. Org. Chem.* 4483-4503.
20. Leroux F (2004) Atropisomerism, biphenyls, and fluorine: A comparison of rotational barriers and twist angles. *ChemBioChem* **5**, 644-649.
21. Muller K, Faeh C, & Diederich F (2007) Fluorine in pharmaceuticals: Looking beyond intuition. *Science* **317**, 1881-1886.
22. Dunitz JD (2004) Organic fluorine: Odd man out. *ChemBioChem* **5**, 614-621.
23. Graupe M, Takenaga M, Koini T, Colorado R, & Lee TR (1999) Oriented surface dipoles strongly influence interfacial wettabilities. *J. Am. Chem. Soc.* **121**, 3222-3223.
24. Merzel F & Smith JC (2002) Is the first hydration shell of lysozyme of higher density than bulk water? *Proc. Natl. Acad. Sci. U. S. A.* **99**, 5378-5383.
25. Pal SK & Zewail AH (2004) Dynamics of water in biological recognition. *Chem. Rev.* **104**, 2099-2123.
26. Levy Y & Onuchic JN (2006) Water mediation in protein folding and molecular recognition. *Annu. Rev. Biophys. Biomol. Struct.* **35**, 389-415.
27. Qiu WH, *et al.* (2006) Protein surface hydration mapped by site-specific mutations. *Proc. Natl. Acad. Sci. U. S. A.* **103**, 13979-13984.
28. Qiu WH, *et al.* (2006) Ultrafast solvation dynamics of human serum albumin: Correlations with conformational transitions and site-selected recognition. *J. Phys. Chem. B* **110**, 10540-10549.
29. Cohen BE, *et al.* (2002) Probing protein electrostatics with a synthetic fluorescent amino acid. *Science* **296**, 1700-1703.

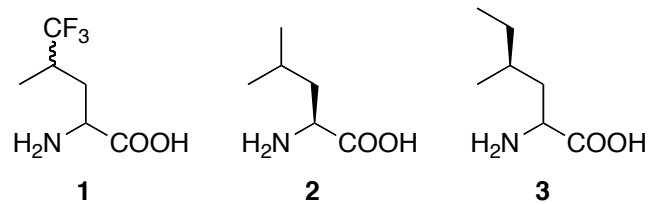
30. Daidone I, Ulmschneider MB, Di Nola A, Amadei A, & Smith JC (2007) Dehydration-driven solvent exposure of hydrophobic surfaces as a driving force in peptide folding. *Proc. Natl. Acad. Sci. U. S. A.* **104**, 15230-15235.
31. Moore FG & Richmond GL (2008) Integration or segregation: How do molecules behave at oil/water interfaces? *Acc. Chem. Res.* **41**, 739-748.
32. Protein variants containing Tfl, Leu, and Hil, are identified by the addition of "-T," "-L," and "-H," respectively. For example, S31L containing Leu is designated "S31L-L."
33. Chen YH, Yang JT, & Martinez HM (1972) Determination of secondary structures of proteins by circular-dichroism and optical rotary dispersion. *Biochemistry* **11**, 4120-4131.
34. Perez-Iratxeta C & Andrade-Navarro MA (2008) K2D2: estimation of protein secondary structure from circular dichroism spectra. *BMC Struct. Biol.* **8**.
35. Petka WA, Harden JL, McGrath KP, Wirtz D, & Tirrell DA (1998) Reversible hydrogels from self-assembling artificial proteins. *Science* **281**, 389-392.
36. Vivian JT & Callis PR (2001) Mechanisms of tryptophan fluorescence shifts in proteins. *Biophys. J.* **80**, 2093-2109.
37. Steiner RF (1991) *Top. Fluoresc. Spectrosc.*, ed Lakowicz JR (Plenum Press, New York), Vol 2, pp 1-52.
38. Qiu WH, *et al.* (2008) Ultrafast quenching of tryptophan fluorescence in proteins: Interresidue and intrahelical electron transfer. *Chem. Phys.* **350**, 154-164.

39. Siemiarczuk A, Petersen CE, Ha CE, Yang JS, & Bhagavan NV (2004) Analysis of tryptophan fluorescence lifetimes in a series of human serum albumin mutants with substitutions in subdomain 2A. *Cell Biochem. Biophys.* **40**, 115-122.
40. Xu JH & Knutson JR (2009) Quasi-static self-quenching of Trp-X and X-Trp dipeptides in water: ultrafast fluorescence decay. *J. Phys. Chem. B* **113**, 12084-12089.
41. Lu WY, Kim J, Qiu WH, & Zhong DP (2004) Femtosecond studies of tryptophan solvation: correlation function and water dynamics at lipid surfaces. *Chem. Phys. Lett.* **388**, 120-126.
42. Li TP, Hassanali AAP, Kao YT, Zhong DP, & Singer SJ (2007) Hydration dynamics and time scales of coupled water-protein fluctuations. *J. Am. Chem. Soc.* **129**, 3376-3382.
43. Zhang LY, Yang Y, Kao YT, Wang LJ, & Zhong DP (2009) Protein hydration dynamics and molecular mechanism of coupled water-protein fluctuations. *J. Am. Chem. Soc.* **131**, 10677-10691.
44. Golosov AA & Karplus M (2007) Probing polar solvation dynamics in proteins: A molecular dynamics simulation analysis. *J. Phys. Chem. B* **111**, 1482-1490.
45. Lee HY, Lee KH, Al-Hashimi HM, & Marsh ENG (2006) Modulating protein structure with fluorinated amino acids: Increased stability and native-like structure conferred on a 4-helix bundle protein by hexafluoroisoleucine. *J. Am. Chem. Soc.* **128**, 337-343.
46. We anticipated that A1m-H would also show hydration dynamics identical to those of A1m-L and A1m-T. However as discussed before, the local protein packing and

flexibility near the Trp probe appear to have been altered by substitution of His for Leu, reflected in the large Trp wobbling angle and total Stokes shift,  $\Delta E_s$ . Because the local structure has been changed, we would expect to observe altered hydration dynamics.

47. Russo D, Hura G, & Head-Gordon T (2004) Hydration dynamics near a model protein surface. *Biophys. J.* **86**, 1852-1862.
48. Russo D, Murarka RK, Copley JRD, & Head-Gordon T (2005) Molecular view of water dynamics near model peptides. *J. Phys. Chem. B* **109**, 12966-12975.
49. Chandler D (2005) Interfaces and the driving force of hydrophobic assembly. *Nature* **437**, 640-647.
50. Richmond GL (2002) Molecular bonding and interactions at aqueous surfaces as probed by vibrational sum frequency spectroscopy. *Chem. Rev.* **102**, 2693-2724.
51. Shen YR & Ostroverkhov V (2006) Sum-frequency vibrational spectroscopy on water interfaces: Polar orientation of water molecules at interfaces. *Chem. Rev.* **106**, 1140-1154.
52. Miller TF, Vanden-Eijnden E, & Chandler D (2007) Solvent coarse-graining and the string method applied to the hydrophobic collapse of a hydrated chain. *Proc. Natl. Acad. Sci. U. S. A.* **104**, 14559-14564.
53. ten Wolde PR & Chandler D (2002) Drying-induced hydrophobic polymer collapse. *Proc. Natl. Acad. Sci. U. S. A.* **99**, 6539-6543.
54. Ashbaugh HS & Paulaitis ME (2001) Effect of solute size and solute-water attractive interactions on hydration water structure around hydrophobic solutes. *J. Am. Chem. Soc.* **123**, 10721-10728.

55. Huang DM & Chandler D (2002) The hydrophobic effect and the influence of solute-solvent attractions. *J. Phys. Chem. B* **106**, 2047-2053.
56. Jensen TR, *et al.* (2003) Water in contact with extended hydrophobic surfaces: Direct evidence of weak dewetting. *Phys. Rev. Lett.* **90**.
57. Mezger M, *et al.* (2010) On the Origin of the Hydrophobic Water Gap: An X-ray Reflectivity and MD Simulation Study. *J. Am. Chem. Soc.* **132**, 6735-6741.
58. Rosky PJ & Dalvi VH (2010) Molecular origins of fluorocarbon hydrophobicity. *Proc. Natl. Acad. Sci. U. S. A.* **107**, 13603-13607.
59. Odonnell MJ & Eckrich TM (1978) Synthesis of amino acid derivatives by catalytic phase transfer alkylations. *Tetrahedron Lett.* 4625-4628.
60. Dorizon P, *et al.* (1999) Stereoselective synthesis of highly functionalized cyclopropanes. Application to the asymmetric synthesis of (1S,2S)-2,3-methanoamino acids. *J. Org. Chem.* **64**, 4712-4724.
61. Swiss Institute of Bioinformatics. Protparam tool. 2003, <http://ca.expasy.org/tools/protparam.html>.
62. Schuck P (2000) Size-distribution analysis of macromolecules by sedimentation velocity ultracentrifugation and Lamm equation modeling. *Biophys. J.* **78**, 1606-1619.
63. Shen XH & Knutson JR (2001) Subpicosecond fluorescence spectra of tryptophan in water. *J. Phys. Chem. B* **105**, 6260-6265.
64. Zhong DP, Pal SK, & Zewail AH (2001) Femtosecond studies of protein - DNA binding and dynamics: Histone I. *Chemphyschem* **2**, 219-227.



Scheme 3.1. Amino acids used in study. **1**, 5,5,5-trifluoroleucine (Tfl). **2**, leucine (Leu). **3**, (4*S*)-2-amino-4-methylhexanoic acid (homoisoleucine, Hil).

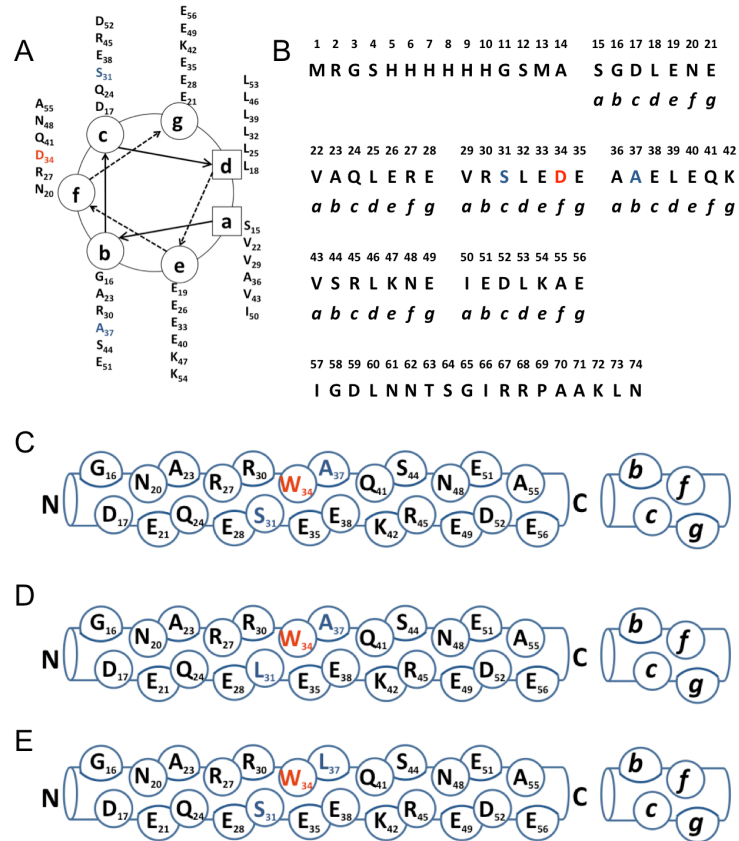


Figure 3.1. Protein sequence and structure. A) Helical wheel diagram and B) amino acid sequence of the A1 protein. The Asp residue at the *f* position of the third heptad (position 34) was replaced by Trp to yield a variant of A1 designated Alm. A Leu codon was introduced at the *c* position of the third heptad (position 31, dark blue) or at the *b* position of the fourth heptad (position 37, dark blue) to yield S31L and A37L, respectively. Side views of C) A1m, D) S31L, and E) A37L.

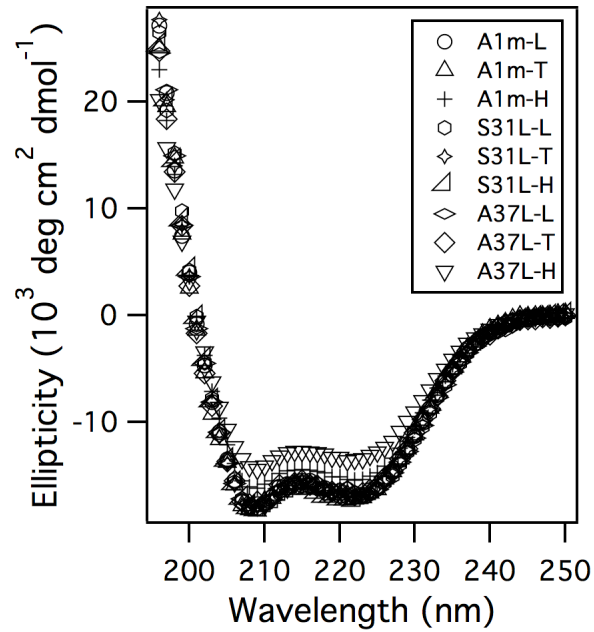


Figure 3.2. Circular dichroism. Wavelength scans of A1m and variant proteins at 25 °C.

The protein samples were prepared at 20  $\mu\text{M}$  concentration in 10 mM acetate (pH 4)/100 mM NaCl solutions.

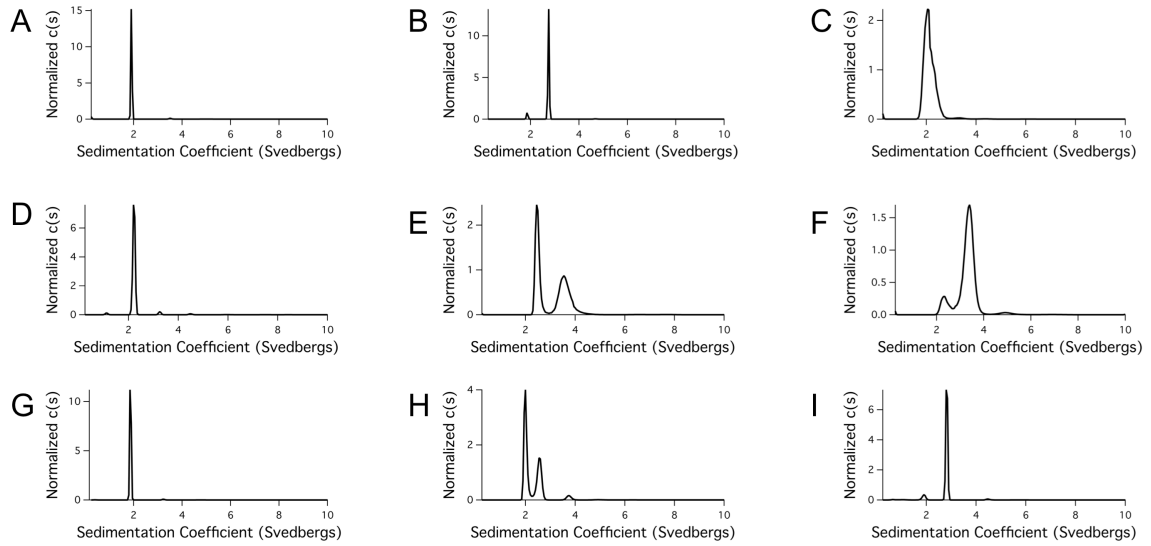


Figure 3.3. Normalized plots from the Sedfit  $c(s)$  analysis for A) A1m-L, B) S31L-L, C) A37L-L, D) A1m-T, E) S31L-T, F) A37L-T, G) A1m-H, H) S31L-H, and I) A37L-H. The protein samples were prepared at 550  $\mu\text{M}$  concentration in 10 mM acetate (pH 4)/100 mM NaCl solution. The broad, single peak of the A37L-L trace may be the result of an equilibrium mixture between trimeric and higher-order species. It seems likely that the breadth of the traces derived from sedimentation velocity analysis of A1m-T, S31L-T, and A37L-T is a consequence of incomplete replacement of Leu with Tfl.

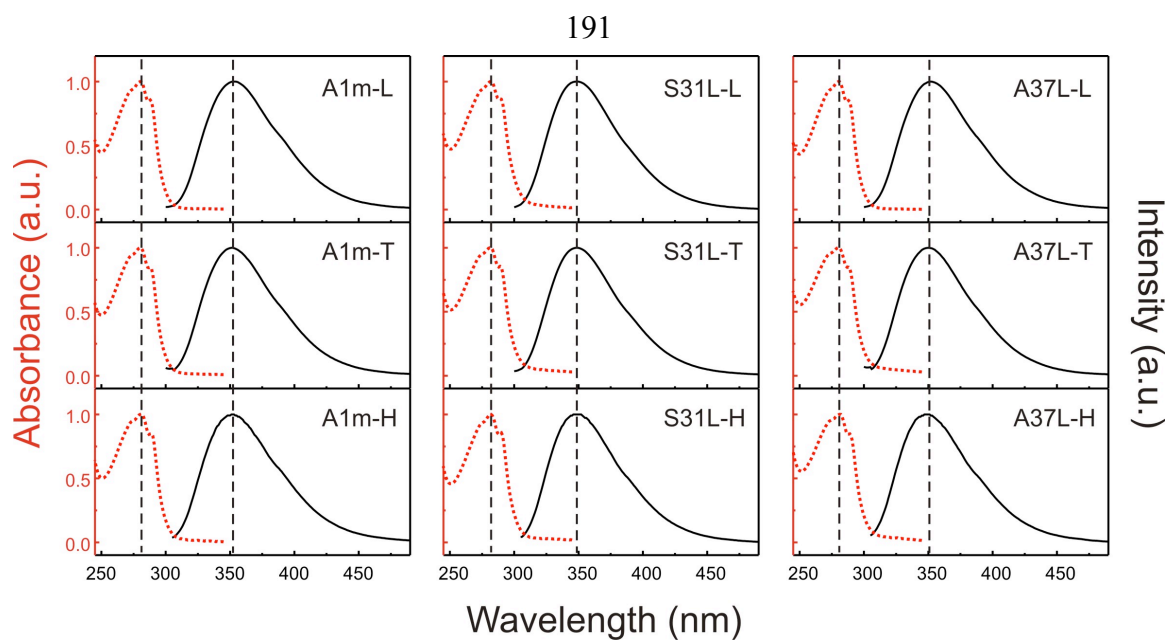


Figure 3.4. Steady-state UV-visible absorption (red) and fluorescence emission spectra (black) of proteins excited at 295 nanometers. The protein samples were prepared at 550  $\mu$ M concentration in 10 mM acetate (pH 4)/100 mM NaCl solution.

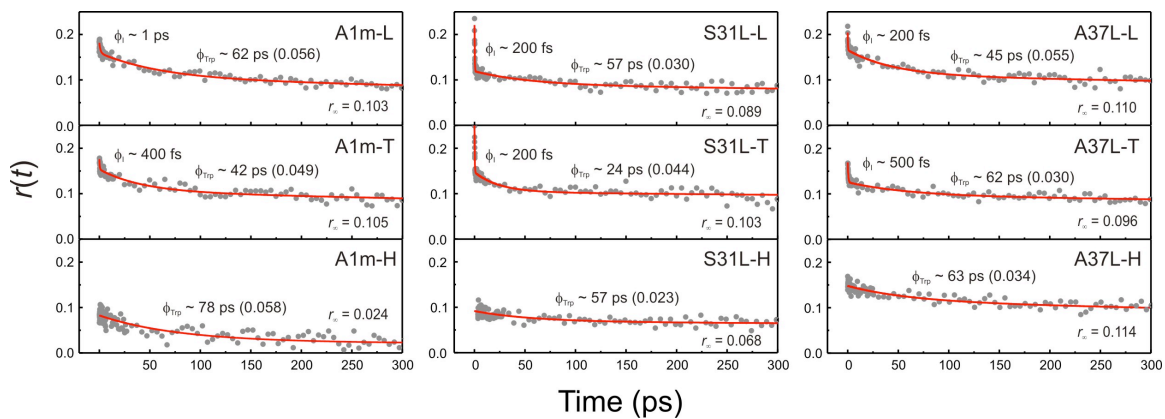


Figure 3.5. Time-resolved anisotropy,  $r(t)$ , of the proteins. All anisotropy decays were fitted to  $r(t) = r_1 \exp(-t/f_1) + r_{\text{Trp}} \exp(-t/f_{\text{Trp}}) + r_\infty$ , where  $r_1$  is the initial ultrafast anisotropy,  $r_{\text{Trp}}$  is the Trp motion-related anisotropy (value given in parentheses in each panel),  $r_\infty$  is the offset anisotropy,  $f_1$  is the initial ultrafast internal-conversion time constant of Trp ( $\leq 1$  ps), and  $f_{\text{Trp}}$  is the Trp-rotational correlation time constant.

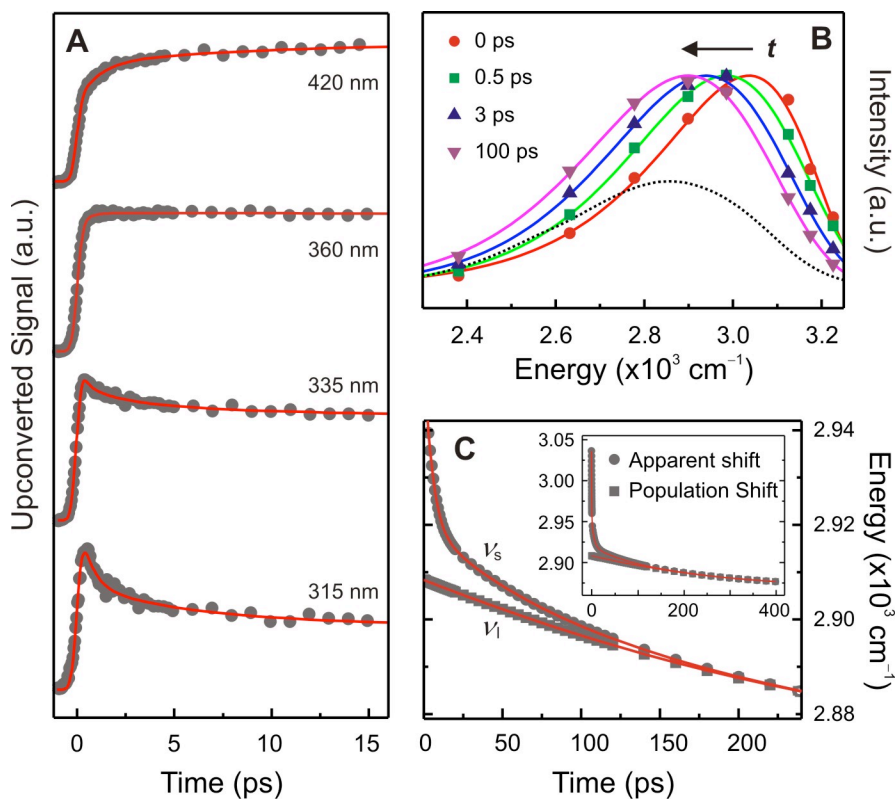


Figure 3.6. Hydration dynamics. Experimental determination of local hydration dynamics at the surface of A1m-T, excited at 295 nm. A) Representative femtosecond-resolved fluorescence up-conversion transients. B) Normalized time-resolved fluorescence spectra at different time delays. The steady-state emission spectrum is also depicted (dotted line). C) Time-dependent spectral shift of the apparent emission maxima ( $\nu_s$ ) and the lifetime-associated (population) emission maxima ( $\nu_l$ ). Inset: entire evolution of  $\nu_s$  and  $\nu_l$ .

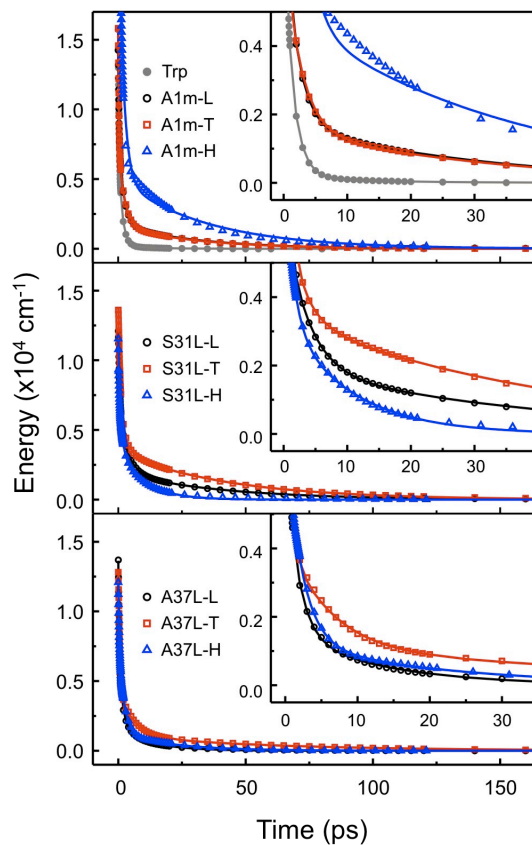


Figure 3.7. Hydration energy relaxation. Comparison of the hydration-correlated energy relaxation,  $\Delta E_s(t)$ , probed by Trp emission. Top panel: The solvation-energy relaxation data for A1m proteins. Data for free Trp in the same buffer is also depicted for comparison. Middle panel: Solvation energy relaxation data for S31L analogs. Bottom panel: solvation energy relaxation data for A37L analogs. Insets: enlargement of the early-time hydration behavior.

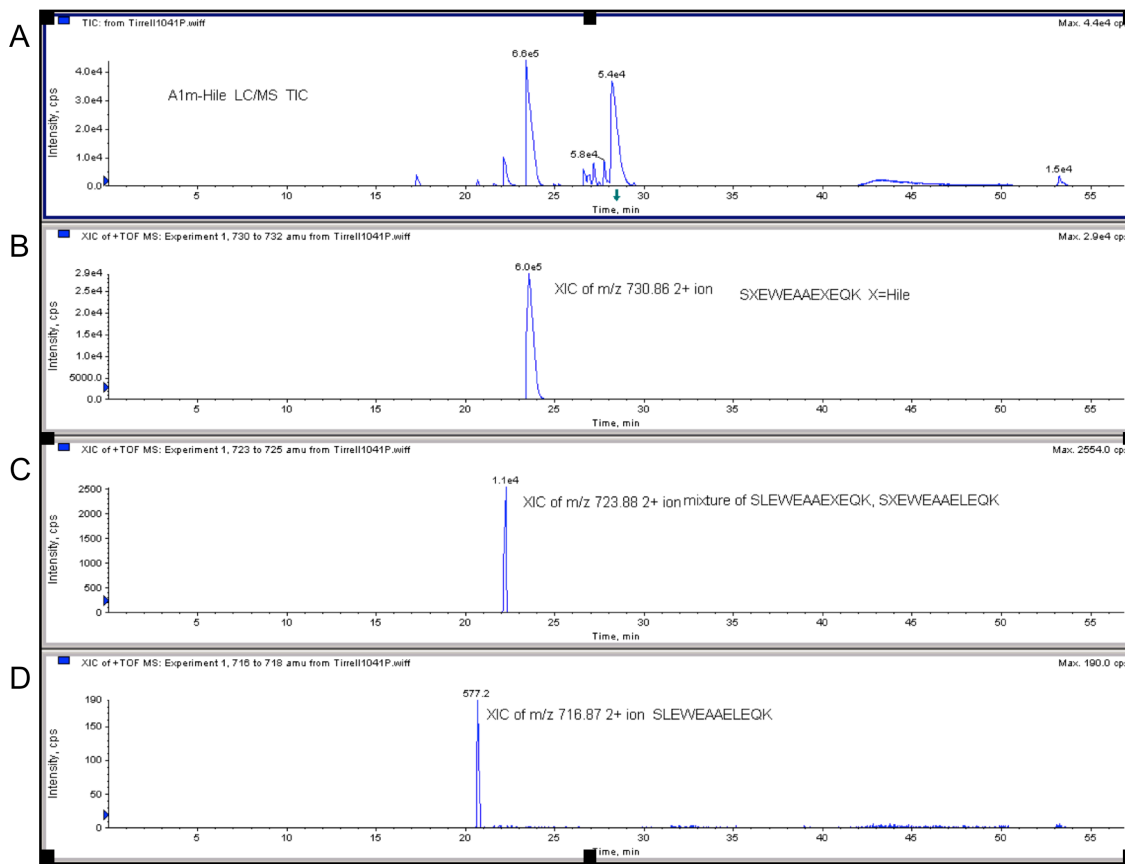


Figure 3.8. LC/MS/MS of trypsinized A1m-H. A) TIC of digested protein sample. B)–D) XICs of peptides containing B) two, C) one, or D) no leucine to homoisoleucine substitutions in the peptide SLEWEEAELEQK. The ratios of the peak areas obtained in the XICs can be used to estimate the extent of leucine replacement in the protein sample. Peptide masses: SXEWEEAEXEQK: 2+ ion: 730.86 Da observed, 730.87 Da expected. SLEWEEAEXEQK, SXEWEEAEXEQK: 2+ ion: 723.88 Da observed, 723.86 Da expected. SLEWEEAELEQK 2+ ion: 716.87 Da observed, 716.85 expected.

Table 3.1. Fluorescence emission maxima ( $\lambda_{\max}$ ), hydration-correlated energy relaxation [ $\Delta E_s(t)$ ], and depolarization dynamics [ $r(t)$ ]

Sample	$\lambda_{\max}$ , nm	$\Delta E_s(t)^*$						$r(t)^\dagger$	
		$\tau_1$ , ps	$\tau_2$ , ps	$\tau_3$ , ps	$E_1$ , $\text{cm}^{-1}$	$E_2$ , $\text{cm}^{-1}$	$E_3$ , $\text{cm}^{-1}$	$r_{\text{Trp}}$	$\theta$ , $^\circ$
Trp	353	0.30	1.5	13	883	682	18	0.196	
A1m-L	352	0.30	2.1	31	610	646	171	0.056	21
A1m-T	352	0.28	2.5	31	877	568	161	0.049	20
A1m-H	352		1.9	34	0	2138	500	0.058	33
S31L-L	349	0.53	3.6	40	580	450	194	0.030	18
S31L-T	349	0.79	3.0	48	607	375	333	0.044	19
S31L-H	349	0.21	1.4	10	308	492	344	0.023	18
A37L-L	352	0.31	1.7	13	685	522	157	0.055	20
A37L-T	350	0.56	6.1	61	685	324	108	0.030	17
A37L-H	349	0.34	2.2	21	443	625	128	0.034	17

\* All hydration-correlated energy relaxation dynamics were fitted to  $\Delta E_s(t) = E_1 \exp(-t/\tau_1) + E_2 \exp(-t/\tau_2) + E_3 \exp(-t/\tau_3)$ .

† Refer to materials and methods for anisotropy analysis detail.